Effect of Nonlinear Gradient Terms on the Dynamics of Solitons in the Cubic-Quintic Complex Ginzburg-Landau Equation

Woo-Pyo Hong

Department of Electronics Engineering, Catholic University of Daegu, Hayang, Gyongsan, Gyungbuk 712-702, South Korea

Reprint requests to Prof. W.-P. H.; E-mail: wphong@cu.ac.kr

The modulational instability of the one-dimensional cubic-quintic complex Ginzburg-Landau equation with the nonlinear gradient terms is investigated. The presence of the nonlinear gradient terms modifies the modulational instability gain spectrum. We numerically investigate the dynamics of modulational instability in the presence of the nonlinear gradient terms. It is found that they introduce more interactions (both elastic and inelastic) dynamics to the solitons generated by the modulational instability. The signs of the gradient terms determine the propagation direction of the soliton. – PACS numbers: 42.65.Tg, 42.81Dp, 42.65.Sf.

Key words: Cubic-Quintic Complex Ginzburg-Landau Equation; Nonlinear Gradient Terms; Modulational Instability; Optical Gain; Soliton; Numerical Simulation.

1. Introduction

It is now well known that a continuous-wave (CW) or quasi-CW radiation propagating in a nonlinear dispersive medium may suffer an instability with respect to weak periodic modulations of the steady-state and results in the breakup of the wave into a train of ultrashort pulses [1]. Modulational instability (MI), occuring as a result of an interplay between the nonlinearity and dispersion (or diffraction, in the spatial domain), is a fundamental and ubiquitous process that appears in most nonlinear wave systems in nature such as fluid dynamics [2,3], nonlinear optics [4,5], and plasma physics [6]. In the context of fiber optics, the temporal MI has been experimentally verified for a single pump wave propagating in a standard non-birefringence fiber, which can be modeled by the nonlinear Schrödinger equation, and it was found that the MI only occurs in anomalous group-velocity dispersion regime with the positive cubic nonlinear term [7].

Recently, Hong [8] has investigated the MI of optical waves in the high dispersive cubic-quintic higher-order nonlinear Schödinger equation. In the more complicated optical systems with the gain and loss terms, described by the cubic-quintic complex Ginzburg-Landau equation, the MI of continuous-wave of the equation has been investigated: The low-amplitude CW solutions are always unstable, meanwhile, for higher-amplitude CW solutions there are regions of stability and regions where they are modulationally unstable [9]. More recently, the effects of the higher order dispersion and gain terms on the dynamics of the solitons induced by the MI in the context of the quintic complex Swift-Hohenberg equation have been investigated by Hong [10], showing that the higher order terms not only modify the MI gain spectrum but also alters the dynamics of the solitons.

In this paper, we investigate the properties of the MI of the extended cubic-quintic complex Ginzburg-Landau equation with the nonlinear gradient terms (NCGLE), which has many important applications in the nonlinear optics and the complicated pattern-forming dissipative systems, in the form [9, 11]

$$
\begin{aligned}
&i\psi_z + \frac{d}{2}\psi_{\tau\tau} + |\psi|^2\psi + (\nu - i\mu)|\psi|^4\psi = \\
&i\delta\psi + i\beta\psi_{\tau\tau} + i\varepsilon|\psi|^2\psi - i\lambda|\psi|^2\psi_\tau - i\kappa\psi^2\psi_\tau^*,
\end{aligned}
\tag{1}
$$

where d, δ, ε, β, μ and λ are real constants. The physical meaning of each particular term depends on the dynamical system under consideration. For example, in the mode-locked laser system, $\psi(z,\tau)$ is the normalized amplitude, z is the propagation distance or the cavity round-trip number (treated as a continuous variable), τ is the retarded time, d is the group-velocity dispersion coefficient with $d = \pm 1$ depending on anomalous ($d = 1$) or normal ($d = -1$) dispersion, δ is the

linear gain ($\delta > 0$) or loss ($\delta < 0$) coefficient, β accounts for spectral filtering or linear parabolic gain ($\beta > 0$) due to an amplifier, the ε term represents the nonlinear gain (which arises, e.g., from saturable absorption), the term with μ represents, if negative, the saturation of the nonlinear gain, and the term with ν coefficients corresponds, if negative, to the saturation of the nonlinear refractive index finally $\lambda = \lambda_r + i\lambda_i$ and $\kappa = \kappa_r + i\kappa_i$ are complex constants related to the effect of self-steepening and self-frequency shift, representing the nonlinear gradient terms [9, 11].

The effects of nonlinear gradient terms on pulsating, erupting and creeping solitons of NCGLE (1) have been analyzed by a numerical method [11]. It was shown that the nonlinear gradient terms result in dramatic changes in the soliton behavior. However, the analysis of the MI gain spectrum and the effects of the nonlinear gradient terms on the evolution of the solitons induced by the MI of NCGLE have not been previously studied, which will be pursued in the present work.

The paper is organized as follows: In Section 2, we obtain the analytic expression for the MI gain spectrum of the NCGLE, study the characteristics of gain in the presence of the nonlinear gradient terms, and compare with those of the CGLE [9]. In Section 3, we numerically investigate the dynamics of the initial steady CW in the anomalous regime under the weak modulational field. In particular, the effect of the nonlinear gradient terms on the final state of MI (solitons) is investigated. The conclusions follow in Section 4.

2. Gain by the Modulational Instability

In order to investigate how weak and time-dependent perturbations evolve along the optical medium described by the NCGLE, we consider the following linear-stability analysis. The steady-state solution of (1) can be given by [1, 8, 10]

$$\bar{\psi}(z,\tau) = A\exp[i\phi_{\mathrm{NL}}(z)], \tag{2}$$

where the linear phase shift $\phi_{\mathrm{NL}}(z)$ is related to the optical amplitude A and the propagation distance z as

$$\phi_{\mathrm{NL}}(z) = zA^2 + z\nu A^4 + i(-z\delta - z\varepsilon A^2 - z\mu A^4). \tag{3}$$

The linear-stability of the steady-state can be examined by introducing the perturbed field of the form

$$\psi(z,\tau) = [A + \eta(z,\tau)]\exp[i\phi_{\mathrm{NL}}(z)], \tag{4}$$

where the complex field $|\eta(z,\tau)| \ll A$. It is obvious that, depending on the strength and sign of the gain or loss terms, i.e., δ, ε, and μ, the steady-state can blow up or decay. However, due to the presence of the perturbed field and its compensation with the steady-state field, one can expect the total field of (4) to be stable and produce non-trivial coherent structures such as solitons, which will be numerically verified in the following section.

By substituting (4) into (1) and collecting the linear terms in η, we obtain the equation for the perturbed field as

$$i\eta_z + [(\nu - i\mu)A^4 + i\delta]\eta + \left(\frac{1}{2}d - i\beta\right)\eta_{\tau\tau}$$
$$+ [(2\nu - 2i\mu)A^4 + (1 - i\varepsilon)A^2]\eta^* \tag{5}$$
$$+ (-\lambda_i + i\lambda_r)A^2\eta_\tau + (-\kappa_i + i\kappa_r)A^2\eta_\tau^* = 0,$$

where $*$ denotes complex conjugate. We assume a general solution of the form

$$\eta(z,\tau) = U\exp[i(Kz - \Omega\tau)]$$
$$+ V\exp[-i(Kz - \Omega\tau)], \tag{6}$$

where K and Ω represent the wave number and the frequency of modulation [1], respectively. Inserting (6) into (5), we obtain the determinant

$$\begin{vmatrix} \Phi^- & \Phi^+ \\ \Lambda^+ & \Lambda^- \end{vmatrix} = 0, \tag{7}$$

where

$$\Phi^\pm = \pm K - \frac{1}{2}d\Omega^2 \pm (\kappa_r - \lambda_r)A^2\Omega + 3\nu A^4 + A^2$$
$$+ i[\beta\Omega^2 \pm (\kappa_i - \lambda_i)A^2\Omega + \delta - \varepsilon A^2 - 3\mu A^4], \tag{8}$$

$$\Lambda^\pm = \beta\Omega^2 + (\lambda_i + \kappa_i)A^2\Omega \pm \mu A^4 \pm \varepsilon A^2 \pm \delta$$
$$+ i[K \pm \frac{1}{2}d\Omega^2 + (-\kappa_r - \lambda_r)A^2\Omega \pm A^2 \pm \nu A^4]. \tag{9}$$

This results in the expression for the wave number K, where

$$K = (\lambda_r + i\lambda_i)\Omega A^2 + \frac{i}{2}\sqrt{K_r + iK_i}, \tag{10}$$

where

$$K_r = (4\beta^2 - d^2)\Omega^4 + \left[(4d\nu + 4\kappa_i^2 - 8\beta\mu - 4\kappa_r^2)A^4 + 8\delta\beta\right]\Omega^2$$
$$+ (12\nu^2 - 12\mu^2)A^8 + (-16\mu\varepsilon + 16\nu)A^6 + (-8\mu\delta + 4 - 4\varepsilon^2)A^4 + 4\delta^2, \tag{11}$$
$$K_i = 4d\Omega^4\beta + \left[(-4\mu d - 8\kappa_i\kappa_r - 8\beta\nu)A^4 + 4d\delta\right]\Omega^2 - 24\nu A^8\mu + (-16\mu - 16\varepsilon\nu)A^6 + (-8\delta\nu - 8\varepsilon)A^4.$$
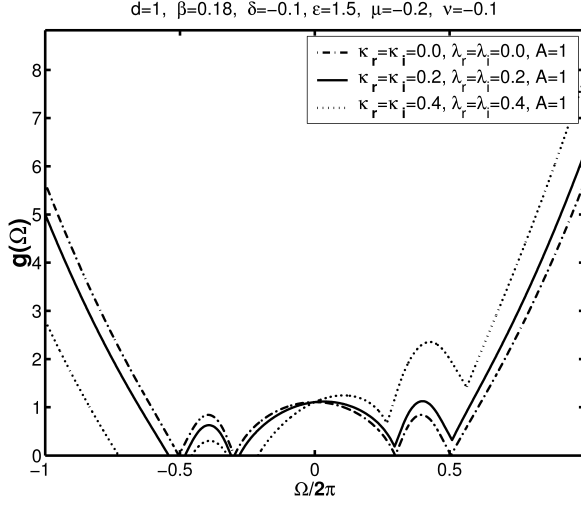

Fig. 1. The gain spectra of the NCGLE show three characteristic peaks. Note the nonzero gain peak at $\Omega = 0$ due to the coefficient terms in K_r and K_i which are independent of Ω in (11). The gain spectra with the nonzero gradient terms (solid and dotted lines) show slightly asymmetric and rapidly increasing gain at $|\Omega/2\pi| > 0.5$ due to the λ_i term, i.e., the dependence of the linear modulation frequency.

Expressing (10) in polar coordinates, we obtain

$$K = (\lambda_r + i\lambda_i)\Omega A^2$$
$$+ \frac{i}{2}[K_r^2 + K_i^2]^{1/4}[\cos(\frac{\theta}{2}) + i\sin(\frac{\theta}{2})], \tag{12}$$

where $\cos(\theta) = K_r/\sqrt{K_r^2 + K_i^2}$. The steady-state solution becomes unstable whenever K has a imaginary part since the perturbation then grows exponentially with the intensity given by the MI gain defined as $g(\Omega) \equiv 2\mathrm{Im}(K)$ [1] as

$$g(\Omega) = 2\lambda_i\Omega A^2$$
$$+ \frac{1}{2}[K_r^2 + K_i^2]^{1/4}\sqrt{2 + 2\cos(\theta)} \tag{13}$$
$$= 2\lambda_i\Omega A^2 + \frac{1}{2}[2\sqrt{K_r^2 + K_i^2} + 2K_r]^{1/2}.$$

The inclusion of the nonlinear gradient terms lets the MI gain spectrum depend on both the linear modulation frequency and the quadratic modulation frequency. Thus, the gain spectrum of (13) indefinitely
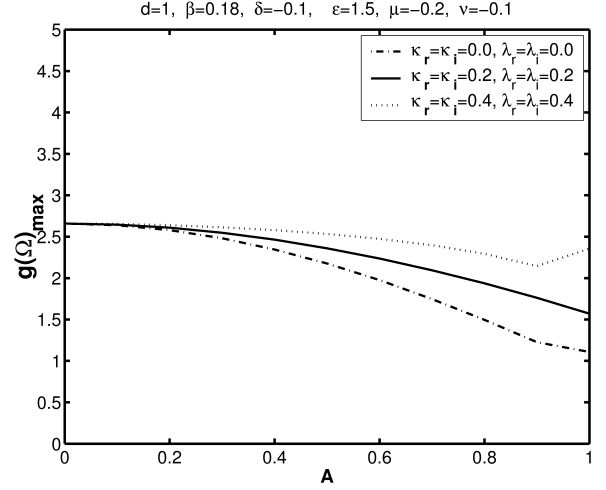

Fig. 2. The maximum gain peak $g(\Omega)_{\mathrm{max}}$ as a function of the amplitude A for the same coefficients as in Fig. 1 with different λ and κ values in the range $|\Omega/2\pi| < 0.5$. Nonzero g_{max} occurs at zero modulation frequency. Note that as λ and κ increases the maximum MI gain also increases

grows as the modulation frequency increases even for a small nonlinear gradient coefficient λ_i. However, at small modulation frequencies the lower orders of Ω terms of K_r and K_i dominate over the highest order Ω. Thus, we expect the similar characteristic MI gain peaks to occur as in [1, 8, 10].

Figure 1 shows the MI gain spectrum $g(\Omega)$ as function of $\Omega/2\pi$ for several values of λ, κ, and the optical amplitude A with the following set of physical coefficients similar to those in [9, 10]: $\beta = 0.18$, $\delta = -0.1$, $\mu = -0.2$, $\nu = -0.1$, and $\varepsilon = 1.5$. For the case of $\kappa = \lambda = 0$, there are three local peaks at low modulational frequencies ($|\Omega/2\pi| < 0.5$). In particular, there exists a nonzero gain peak at $\Omega/2\pi = 0$ due to the coefficient terms in K_r and K_i in (11) which are independent of Ω. However, the gain spectra of NCGLE (solid and dotted curves) show slightly asymmetric and rapidly increasing gain at $|\Omega/2\pi| > 0.5$ due to the λ_i term, i.e., the dependence of the linear modulation frequency. Figure 2 shows the dependence of the maximum gain $g(\Omega)_{\mathrm{max}}$ on A for the same coefficients as in Fig. 1 in the range $|\Omega/2\pi| < 0.5$. The maximum gain of the NCGLE (solid and dashed curves) in Fig. 2 in-
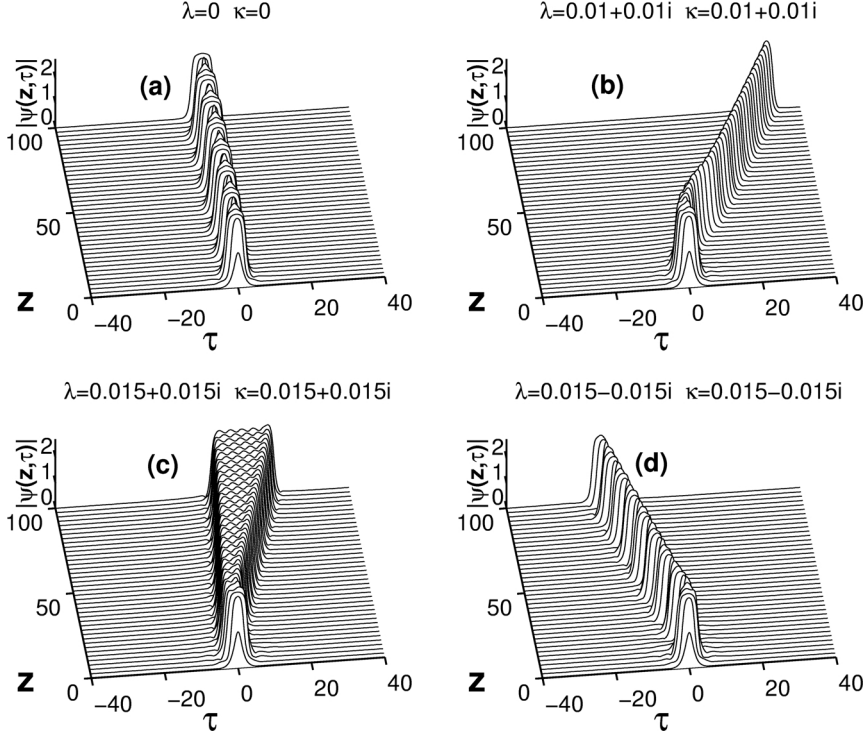
Fig. 3. Effect of the nonlinear gradient terms on the pulsating soliton. The set of coefficients used is $\beta = 0.08$, $\delta = -0.1$, $\mu = -0.1$, $v = -0.1$, and $\varepsilon = 0.66$ with the initial profile $\psi(0, \tau) = \mathrm{sech}(\tau)$. (a) Evolution of the pulsating soliton for $\lambda = \kappa = 0$. (b) Evolution of the soliton which travels toward the right by maintaining a stable fixed-shape without showing pulsation for $\lambda = \kappa = 0.01 + 0.01i$. (c) Evolution of the initial soliton to a front for $\lambda = \kappa = 0.015 + 0.015i$. (d) Evolution of the pulsating soliton but traveling toward the left for $\lambda = \kappa = 0.015 - 0.015i$.

creases with A as the strength of the nonlinear gradient terms increases.

Before we proceed to the numerical simulations of the MI, it is worth noting that the wave number K in (12) has not only the purely growing imaginary term but also the real term, giving an oscillatory instability, which may influence to a solitary-wave formation at the end process of MI. As shown in (4), due to the exponentially decaying ($\delta < 0$, $\varepsilon > 0$, and $\mu < 0$ in this work) or increasing factor can modify (13), therefore, the effective gain is given as

$$g_{\mathrm{eff}}(\Omega) = (\delta + \varepsilon A^2 + \mu A^4) + 2\lambda_i \Omega A^2 \\ + \frac{1}{2}[2\sqrt{K_r^2 + K_i^2} + 2K_r]^{1/2}, \qquad (14)$$

which only shifts the magnitude of (13).

3. Numerical Simulations

In order to understand the dynamics of a CW under the MI, (1) is solved, utilizing the split-step Fourier method applying the periodic boundary condition [10, 12]. We use an incident field at the launch plane $z = 0$ into the nonlinear medium of the form

$$\psi(0, \tau) = [A + \varepsilon_{\mathrm{m}} \cos(\Omega_{\mathrm{m}}\tau)], \qquad (15)$$

where ε_{m} is the strength of the modulation amplitude and Ω_{m} is the angular frequency of a weak sinusoidal modulation imposed on the CW, which can be determined from the gain spectra for the given set of coefficients such as in Figure 1. Among many sets of possible coefficients of (1), in this section, we only focus on the effects of κ and λ terms to the evolution of MI.

Before investigating the effects of the nonlinear gradient terms on the dynamics of the soliton generated by the MI, we simulate in Fig. 3 the evolution of the initial soliton, in the form of $\psi(0, \tau) = \mathrm{sech}(\tau)$, for different nonlinear gradient coefficients to investigate how they affect the soliton dynamics. For the following calculations, we set the coefficients as $\beta = 0.08$, $\delta = -0.1$, $\mu = -0.1$, $v = -0.1$, and $\varepsilon = 0.66$. We find in Fig. 3a the typical 'pulsating' soliton which is previously found in [9]. As previously investigated by Tian et al. [11] for the case of $\kappa_r = \kappa_i = 0.01$ and $\lambda_r = \lambda_i = 0.01$, we observe in Fig. 3b the drastic changes in the soliton behavior: traveling toward the right by maintaining a stable fixed-shape without showing pulsating pattern. For the case of $\kappa_r = \kappa_i = 0.015$ and $\lambda_r = \lambda_i = 0.015$, the evolution of the initial soliton to a front is shown in Figure 3c. However, for the case
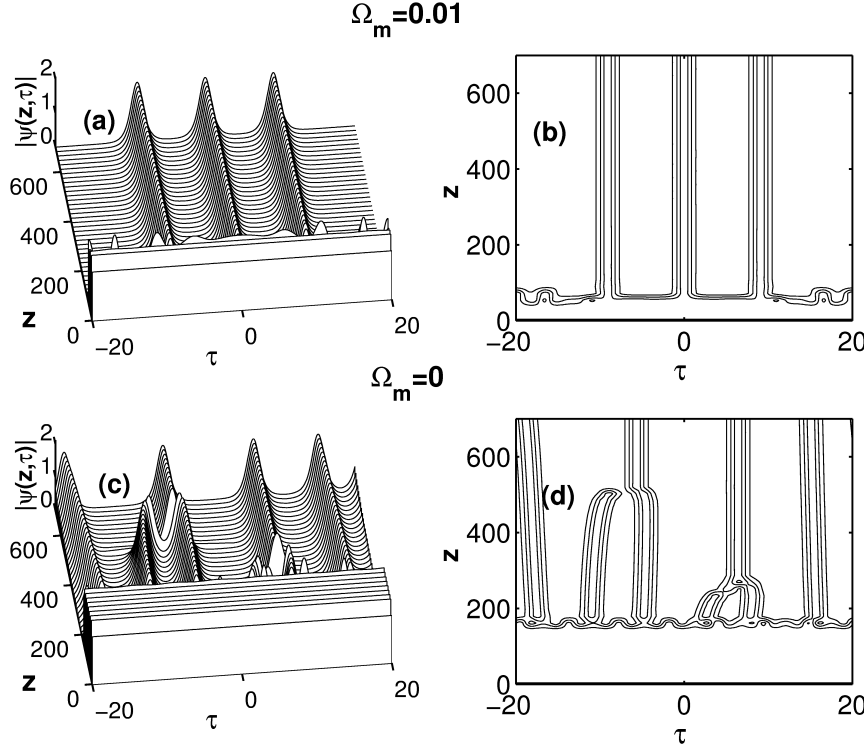
Ω_{m}=0.01

Ω_{m}=0

Fig. 4. Simulations of an injected CW to the nonlinear medium supporting anomalous dispersion with $\beta = 0.18$, $\delta = -0.1$, $\mu = -0.2$, $v = -0.1$, and $\varepsilon = 0.35$ for two modulation frequencies. Note that the nonlinear gradient terms are absent. (a) Evolution of the MI induced solitons for $\Omega_{\mathrm{m}} = 0.01$ and $\varepsilon_{\mathrm{m}} = 0.01$. (b) Contour plot of (a). The stability of the solitons is clearly demonstrated. (c) Evolution of the MI induced solitons for $\Omega_{\mathrm{m}} = 0.01$ an $\varepsilon_{\mathrm{m}} = 0.01$. Note that the distance at which the MI generates the soliton occurs at longer z approximately at $z \approx 180$. (d) Contour plot of (c). Highly inelastic interactions occur at $z \approx 230$ and $z \approx 500$, after which the stability of solitons is maintained.

of $\kappa_r = -\kappa_i = 0.015$ and $\lambda_r = -\lambda_i = 0.015$, we find in Fig. 3d the usual pulsating soliton similar to Fig. 3a but traveling toward the left. It is easy to conclude that the sign of the imaginary nonlinear gradient terms governs the direction of the soliton propagation, while the real nonlinear gradient terms deal with the shape of the soliton.

We calculate the evolution of the MI in Fig. 4 in the absence of the nonlinear gradient terms for an injected CW to the nonlinear medium supporting anomalous dispersion ($d = 1$) by choosing, as an example, $\beta = 0.18$, $\delta = -0.1$, $\mu = -0.2$, $v = -0.1$, $\varepsilon = 0.35$, and the perturbed field amplitude $\varepsilon_{\mathrm{m}} = 0.01$. Figure 4a shows an occurrence of several unstable peaks for $\Omega_{\mathrm{m}} = 0.01$ which subsequently develop to the solitons through the MI. In particular, three solitons generated from the modulated field show stable propagation without mutual interaction, which is clearly demonstrated in the contour plot of Figure 4b. An interesting fact in Fig. 4d is that the number of the modulationally unstable peaks increases when a constant CW amplitude, i.e., $\psi(0,\tau) = A + \varepsilon_{\mathrm{m}}$ for zero modulation frequency, where $A = 1$, is applied. The reason is that not only the MI gain exists at $\Omega_{\mathrm{m}} = 0$, but also it has the bigger value than that at $\Omega_{\mathrm{m}} = 0.01$ according to Fig-

ure 1. On the other hand, in comparison with Fig. 4a, the distance at which the soliton is generated through the MI at $\Omega_{\mathrm{m}} = 0$, increases. The highly inelastic interactions are shown to occur in the contour plot of Fig. 4d at $z \approx 230$ and $z \approx 500$, after which the stability of solitons is maintained.

The effect of the nonlinear gradient terms on the dynamics of the solitons generated by the MI for $\Omega_{\mathrm{m}} = 0.01$ and $\Omega_{\mathrm{m}} = 0$ are shown in Figs. 5 and 7, respectively, by taking $\beta = 0.18$, $\delta = -0.1$, $\mu = -0.2$, $v = -0.1$, $\varepsilon = 0.45$, and $\varepsilon_{\mathrm{m}} = 0.01$. Fig. 5a, where small gradient terms are introduced, shows that modulationally unstable peaks develop to the solitons which interact inelastically during their propagations, for example, at $z \approx 160$. Further increase in the strength of the nonlinear gradient terms, as shown in Figs. 5b and c, not only increase the MI gain values but also the gradient terms act as an effective interaction potential for the solitons generated by the MI. As the consequences, more modulationally unstable peaks appear, the occurrence of inelastic interactions increases, and the velocity of the stably propagating soliton toward the left increases. Lastly, for $\lambda_r = \lambda_i = 0.025$ and $\lambda_r = \lambda_i = 0.025$, we find in Fig. 5d that positive imaginary gradient terms make the soliton propagate
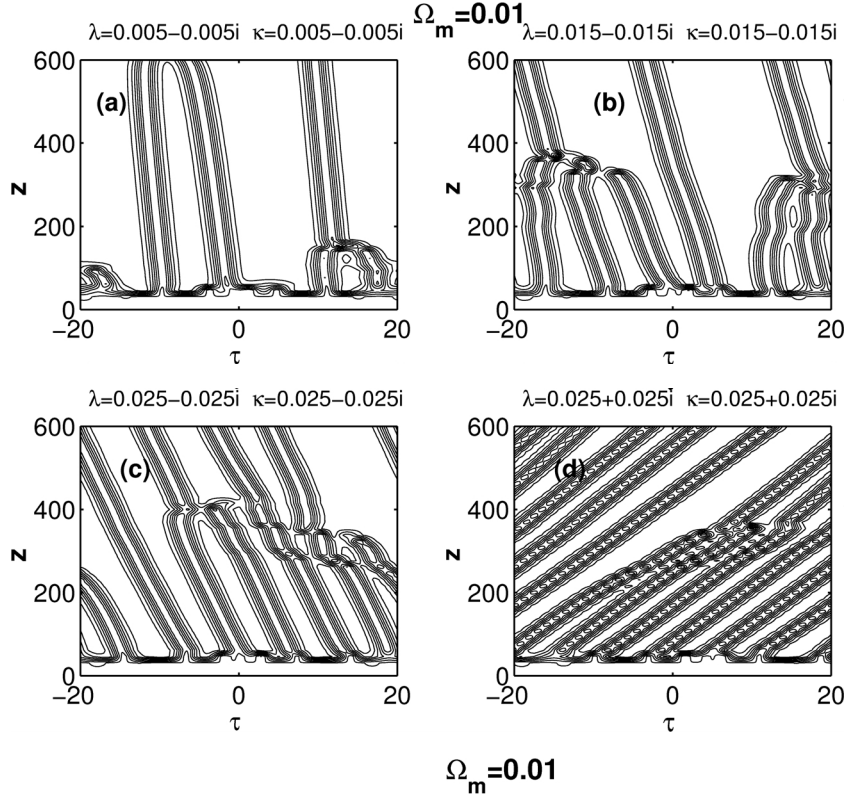
Fig. 5. Contour plots of the MI evolution showing the effects of the nonlinear gradient terms on the dynamics of solitons. The set of coefficient used are $\beta = 0.18$, $\delta = -0.1$, $\mu = -0.2$, $\nu = -0.1$, $\varepsilon = 0.45$, and $\varepsilon_{\mathrm{m}} = 0.01$. (a) MI develops into the solitons which show the strong inelastic interaction at $z \approx 160$. (b) Two inelastic collisions result in the stable soliton propagation. (c) Series of inelastic interactions occur and the velocity of the soliton propagating toward the right increases. (d) The positive imaginary gradient terms make the soliton propagate toward the right while the real gradient terms increase the number of interactions.
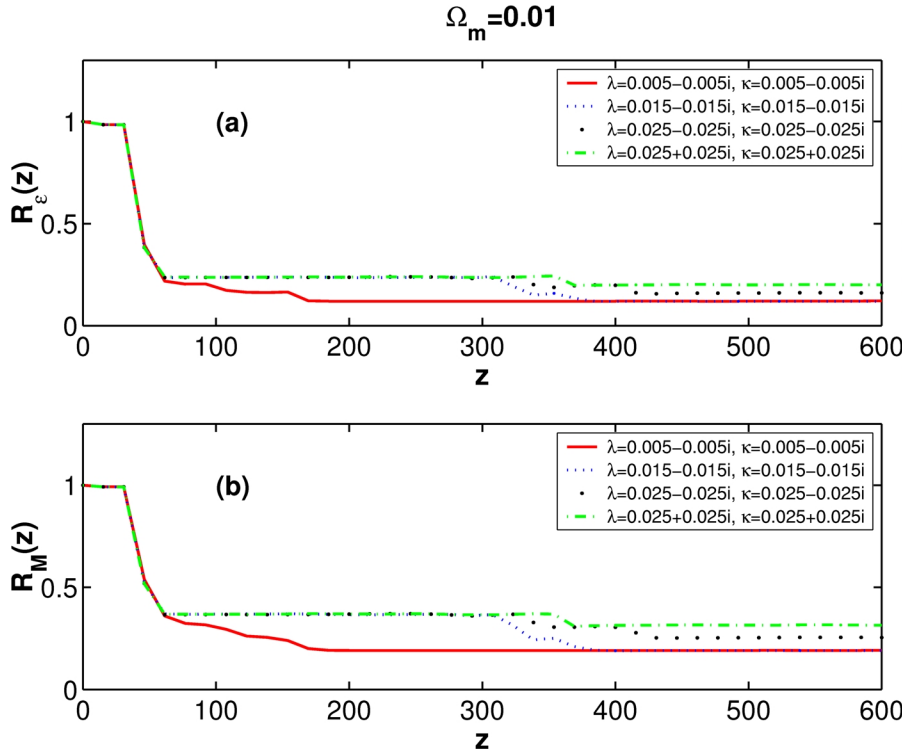

Fig. 6. (a) Evolution of the normalized energy for Figs. 5a–d. The first drop from the initial value at $z \approx 40$ for $\lambda = \kappa = 0.005$ (solid line) corresponds to the distance where the solitons are generated by the MI. The distances where the inelastic interaction occurs are at $z \approx 80$ and at $z \approx 160$. The stability of the soliton is indicated by the flat line. (b) Evolutions of the normalized mass for Figs. 5a–d. Similar behavior as in (a) is observed.
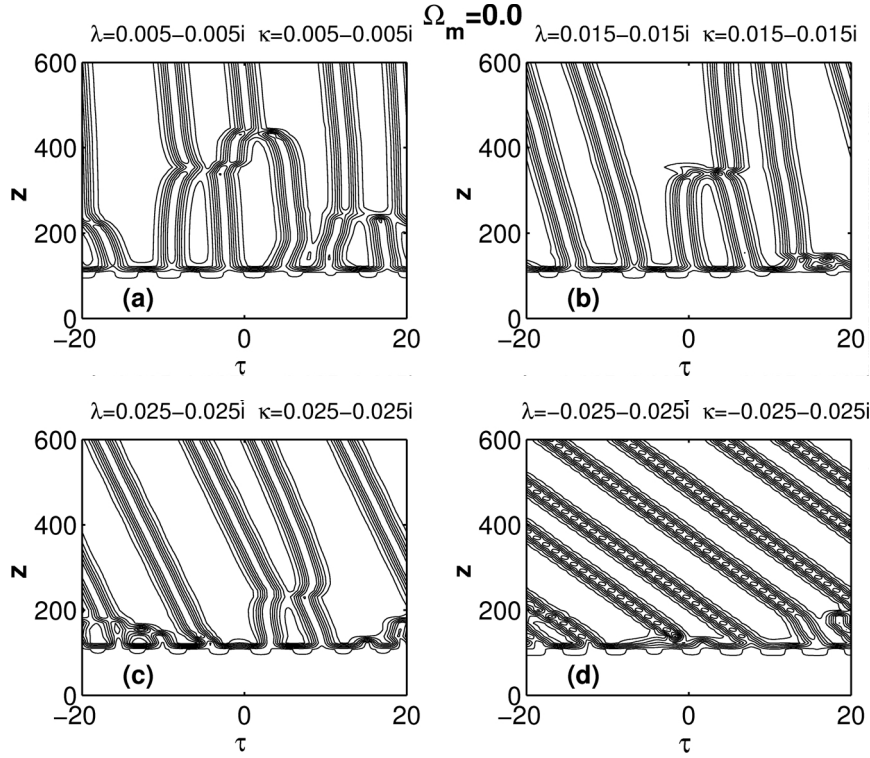
Fig. 7. Contour plots of the MI evolution showing the effects of the nonlinear gradient terms on the dynamics of the solitons. The same set of coefficients as in Fig. 5 except $\Omega_{\mathrm{m}} = 0$ is used. (a) Small nonlinear gradient terms lead to complicated dynamical patterns. The elastic scattering at $z \approx 240$ and the fusion of two solitons into a stable soliton after the inelastic interaction at $z \approx 440$ are shown. (b) The fusion of solitons at $z \approx 300$ is found. (c) The elastic scattering at $z \approx 220$ occurs. (d) For negative imaginary gradient terms, the solitons propagate to the left.

toward the right while still showing inelastic interaction at $z \approx 300$.

Dynamical properties of the MI and the evolution of solitons can be more thoroughly investigated from the energy and mass (or the area under $|\psi(z,\tau)|$) defined as follows:

$$\mathcal{E}(z) \equiv \int_{-\infty}^{\infty} |\psi(z,\tau)|^2 \mathrm{d}\tau,$$

$$M(z) \equiv \int_{-\infty}^{\infty} |\psi(z,\tau)| \mathrm{d}\tau. \tag{16}$$

In Fig. 6 the evolutions of the normalized energy $R_{\mathcal{E}}(z) \equiv \mathcal{E}(z)/\mathcal{E}(0)$ and the normalized mass $R_M(z) \equiv M(z)/M(0)$, respectively, for Fig. 5 calculated. For weak nonlinear gradient terms, both the normalized energy and mass (solid lines) in Figs. 6a and b, respectively, show the first sudden drop from the initial values at $z \approx 40$ corresponding to the solitons generation by the MI as shown in Figure 5a. The subsequent drops correspond to the occurrence of the inelastic interaction at $z \approx 80$ and at $z \approx 180$, after which the solitons propagate stably as indicated by the flat line. The decreases in the normalized energy mean that the evolution of the MI and the inelastic interaction process are not energy conserving. On the other hand,

in the presence of stronger nonlinear gradient terms, both the normalized energy and mass (dashed, dotted, and dot-dashed curves) show sudden drops similar to Fig. 6, however, the energy variation is smaller than the weaker gradient terms (solid line). Thus, we conclude that the presence of the nonzero gradient terms not only result in more interactions between the solitons but also in combination of other nonlinear terms (δ, ε, $\mu < 0$); they act as an effective energy loss or gain term.

We now consider the case $\Omega_{\mathrm{m}} = 0$ in the presence of the nonlinear gradient terms. In Fig. 7, the dynamics of the solitons using the same set of coefficients of Fig. 5 are shown. When small gradient terms are added, more complicated dynamical patterns appear in Fig. 7a such as the elastic scattering at $z \approx 240$ and the fusion of two solitons into a stable one after the inelastic interaction at $z \approx 440$. However, with stronger nonlinear gradient terms, the fusion of solitons at $z \approx 300$ in Fig. 7b and the elastic scattering at $z \approx 220$ in Fig. 7c appears. The fact that the sign of λ_i and κ_i determines the propagation direction of the soliton is clearly shown in Fig. 7d, where the soliton propagate to the left. On the other hand, the normalized energy and mass evolutions for $\Omega_{\mathrm{m}} = 0$ in Figs. 8a and b, respectively, show
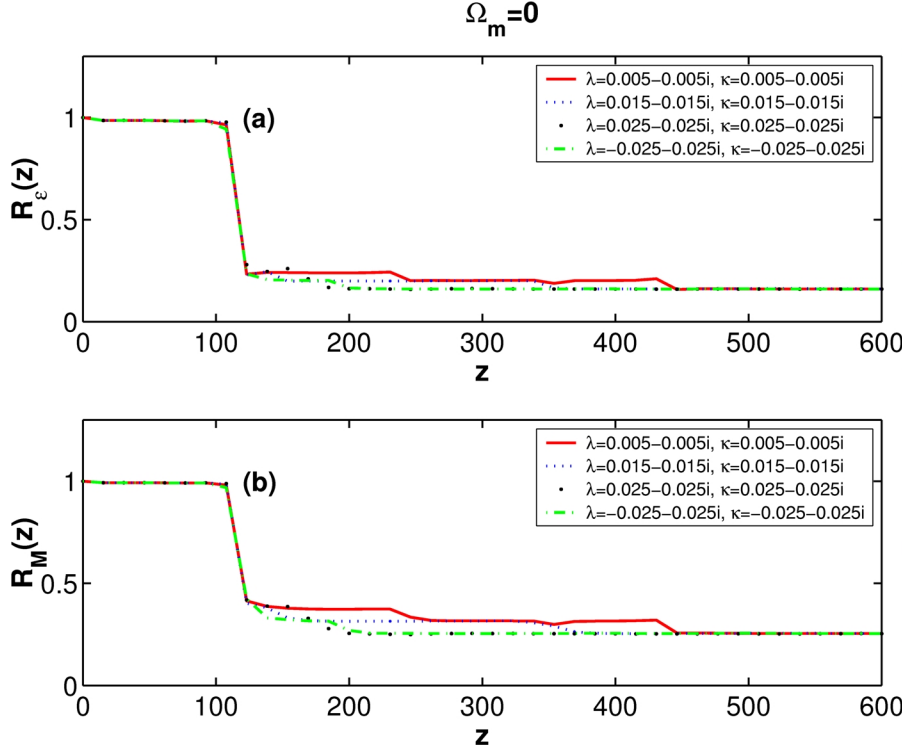
$\Omega_m = 0$

Fig. 8. (a) Evolution of the normalized energy for Figs. 7a – d. The first drop at $z \approx 100$ for $\lambda = \kappa = 0.005$ (solid line) corresponds to the distance where the solitons are generated by the MI. The distances where the inelastic interactions take place are at $z \approx 240$ and at $z \approx 440$. The stability of the soliton is indicated by the flat line. (b) Evolution of the normalized mass for Figs. 7a – d. Similar behavior as in (a) is observed. Note that the energy and mass do not deviate much from each other as λ and κ increase.

the similar variations as the case $\Omega_m = 0.01$ in Fig. 6 except that the soliton by the MI is generated at longer distance and the energy and mass do not deviate much from each other as λ and κ increase.

4. Conclusions

In this work, we have derived the analytic expression for the MI gain of (1), which is an extended model of the cubic-quintic complex Ginzburg-Landau equation by adding the nonlinear gradient terms. It was shown that the presence of the nonlinear gradient terms changes the characteristic MI gain spectrum of the CGLE as shown in Figure 1. The presence of the gradient terms makes the MI gain spectrum depend on the linear modulation frequency term at larger frequency range and allows nonzero MI gain at zero modulation frequency. The maximum gain spectra shown in Fig. 2 are different from those of [9, 10] in that all CWs for the given particular set of coefficients are always unstable even at zero modulation frequency.

The fact that the nonlinear gradient terms can change the shape and the propagation direction of the

soliton has been numerically demonstrated in Fig. 3, using the split-step Fourier method, in agreement with the results in [11]. The dynamics of modulationally unstable CW in the presence of the nonlinear gradient terms has been analyzed in Figs. 5 and 7 for $\Omega_m = 0.01$ and $\Omega_m = 0$, respectively. The gradient terms effect on the dynamics of the MI generated solitons by increasing both the inelastic interaction (fusion of solitons to a stable one) in Fig. 5a and the elastic scattering in Figure 7a. The propagation direction of the MI induced soliton is determined by the sign of the imaginary gradient terms as shown in Figs. 5d and 7d. On the other hand, their effects to the energy and mass have been calculated in Figs. 6 and 8, showing the sudden drops from the initial values while the MI developing into the solitons and their subsequent interactions. It has been also demonstrated that the solitons generated by the MI and the inelastic interaction are the energy dissipating processes.

[1] G. P. Agrawal, Nonlinear Fiber Optics (Optics and Photonics), Academic Press, New York 2001.

[2] G. B. Whitham, Proc. Roy. Soc. **283**, 238 (1965).

[3] T. B. Benjamin and J. E. Feir, J. Fluid Mech. **27**, 417 (1967).

[4] V. I. Bespalov and V. I. Talanov, JETP Lett. **3**, 307 (1966).

[5] V. I. Karpman, JETP Lett. **6**, 277 (1967).

[6] T. Taniuti and H. Washimi, Phys. Rev. Lett. **21**, 209 (1968).

[7] K. Tai, A. Hasegawa, and A. Tomita, Phys. Rev. Lett. **56**, 135 (1986).

[8] W. P. Hong, Opt. Commun. **213**, 178 (2002).

[9] J. M. Soto-Crespo, N. Ahkmediev, and G. Town, J. Opt. Soc. Am. B **19**, 234 (2002).

[10] W. P. Hong, Z. Naturforsch. **59a**, 437 (2004).

[11] H. P. Tian, Z. H. Li, J. P. Tian, G. S. Zhou, and J. Zi, Appl. Phys. B **78**, 199 (2004).

[12] J. A. C. Heideman and B. M. Herbst, SIAM J. Numer. Anal. **23**, 485 (1986).